Author(s): Procter, M.G.; Cullen, David; Scholey, Catherine; Ruotsalainen, Panu; Angus, L.; Bäck, Torbjörn; Cederwall, Bo; Dewald, A.; Fransen, C.; Grahn, Tuomas; Greenlees, Paul; Hackstein, M.; Jakobsson, Ulrika; Jones, Peter; Julin, Rauno; Juutinen, Sakari; Ketelhut, Steffen; Leino, Matti; Liotta, R.; Lumley, N.M.; Mason, P.J.R.; Nieminen, Päivi; Nyman, Markus; Pakarinen, Janne; Pissulla, T.; Peura, Pauli; Rahkila, Panu; Revill, J.; Rigby, Sarah; Rother, W.; Sandzelius, Mikael; Saren, Jan; Sorri, Juha; Taylor, M.J.; Uusitalo

Title: Electromagnetic transition strengths in 109Te

Year: 2012

Version:

Please cite the original version:

Procter, M.G., Cullen, D., Scholey, C., Ruotsalainen, P., Angus, L., Bäck, T., Cederwall, B., Dewald, A., Fransen, C., Grahn, T., Greenlees, P., Hackstein, M., Jakobsson, U., Jones, P., Julin, R., Juutinen, S., Ketelhut, S., Leino, M., Liotta, R., . . . Xu, F.R. (2012). Electromagnetic transition strengths in 109Te. Physical Review C, 86(3), 034308. https://doi.org/10.1103/PhysRevC.86.034308

Electromagnetic transition strengths in $^{109}_{52}$Te

M. G. Procter,[1,*] D. M. Cullen,[1,†] C. Scholey,[2] P. Ruotsalainen,[2] L. Angus,[3] T. Bäck,[4] B. Cederwall,[4] A. Dewald,[5] C. Fransen,[5] T. Grahn,[6,‡] P. T. Greenlees,[2] M. Hackstein,[5] U. Jakobsson,[2] P. M. Jones,[2,§] R. Julin,[2] S. Juutinen,[2] S. Ketelhut,[2] M. Leino,[2] R. Liotta,[4] N. M. Lumley,[1] P. J. R. Mason,[1] P. Nieminen,[2] M. Nyman,[2,‖] J. Pakarinen,[6,‡] T. Pissulla,[5] P. Peura,[2] P. Rahkila,[2] J. Revill,[6] S. V. Rigby,[6] W. Rother,[5] M. Sandzelius,[2] J. Sarén,[2] J. Sorri,[2] M. J. Taylor,[1] J. Uusitalo,[2] P. Wady,[3] C. Qi,[4] and F. R. Xu[7]

[1]*Schuster Laboratory, University of Manchester, Manchester M13 9PL, United Kingdom*
[2]*Department of Physics, University of Jyväskylä, FIN-40014 Jyväskylä, Finland*
[3]*University of the West of Scotland, High Street, Paisley PA1 2BE, United Kingdom*
[4]*Department of Physics, Royal Institute of Technology, SE-10691 Stockholm, Sweden*
[5]*Institut für Kernphysik, Universität zu Köln, D-50937, Köln, Germany*
[6]*Oliver Lodge Laboratory, University of Liverpool, Liverpool L69 7ZE, United Kingdom*
[7]*Department of Technical Physics, Peking University, Beijing 100871, China*

(Received 2 August 2012; published 7 September 2012)

Lifetime measurements have been made in the neutron-deficient nucleus ^{109}Te using the coincident recoil distance Doppler-shift method. The experimental $B(E2)$ values have been compared with state-of-the-art shell-model calculations using the monopole-corrected realistic charge-dependent Bonn nucleon-nucleon potential. Lifetimes in the $\nu h_{11/2}$ band are consistent with an interpretation based on the deformation driving properties of a single valence neutron outside of the even-even tellurium core and highlight the unexpected presence of collective behavior as the $N = 50$ shell closure is approached. Lifetime measurements for the low-lying positive-parity states also appear to correlate well with shell-model calculations. In addition, a comparison with the proton-unbound nucleus ^{109}I suggests that the presence of a single decoupled valence proton affects the total measured $B(E2)$ strengths in a manner that is not currently well understood.

DOI: 10.1103/PhysRevC.86.034308 PACS number(s): 21.10.Tg, 21.60.Cs, 23.20.−g, 27.60.+j

I. INTRODUCTION

The experimental study of excited-state lifetimes in nuclei near the doubly-magic $N = Z = 50$ shell gaps has started to provide a new testing ground for theoretical shell-model calculations around the proton drip line. In this region of the nuclear chart the $d_{5/2}$, $g_{7/2}$ and $h_{11/2}$ single-particle orbitals are observed experimentally in many of the neutron-deficient odd-A nuclei, for example, Refs. [1–3]. In particular, in the neutron-deficient odd-mass $Z = 52$ tellurium isotopes, band structures built upon these shell-model orbits provide some of the best examples of evolving nuclear collectivity in a system comprising only a handful of valence nucleons [4–7]. Extensive spectroscopic studies of the even-mass tellurium nuclei have highlighted the importance of residual interactions between the valence nucleons and the ^{100}Sn core [8]. Deviations have been observed from the expected trend of increasing 2^+ excitation energies as the $N = 50$ shell closure is approached. For $N < 62$ the behavior of the experimental level energies gives evidence for an increase in collectivity and it is only when the $N = 54$, ^{106}Te isotope is reached, the most neutron-deficient tellurium isotope identified to date, that a more expected seniority-like level scheme is observed. Such behavior has been suggested to result from the increasing contribution of the $T = 0$ isoscalar component of the nucleon-nucleon interaction [9]. However, more recent calculations [10] were able to account for many of the observed structural effects in most neutron-deficient xenon isotopes without the need for $T = 0$ pairing.

In order to reveal the underlying reasons for a changing nuclear structure, systematic studies across an entire isotopic chain of a particular nuclear species are generally required. However, useful information for a single nucleus can still be gained from the measurement of experimental γ-ray transition strengths, especially at the extremes of existence. As an example, the $T_z = 5/2$ nucleus ^{109}Te, with seven valence neutrons, provides an accessible platform from which the observed trends in neutron-deficient tellurium isotopes can be explored. In this article the results of an experiment performed at the University of Jyväsklä are reported. The primary aim of the experiment was the study of the lifetimes of excited states in the proton-unbound nucleus ^{109}I [11,12]. The results presented here focus on the $2pn$ exit channel ^{109}Te from the same fusion-evaporation reaction. Reduced transition probabilities have been determined from experimental lifetime measurements using the recoil distance Doppler-shift technique (RDDS) [13]. The results have been compared to state-of-the-art shell-model calculations in order to assess the changes in nuclear structure as the $N = Z = 50$ shell closure is approached.

*mark.procter@manchester.ac.uk
†On leave at the Department of Physics, University of Jyväskylä, FIN-40014 Jyväskylä, Finland.
‡Present address: Department of Physics, University of Jyväskylä, FIN-40014 Jyväskylä, Finland.
§Present address: Department of Nuclear Physics, iThemba Labs, Somerset West 7219, South Africa.
‖Present address: Department of Physics, University of Helsinki, FIN-00014 Helsinki, Finland.

II. EXPERIMENTAL METHODS

An RDDS experiment was performed with the Köln plunger device at the K130 Accelerator Laboratory at the University of Jyväskylä, Finland. Excited states in ^{109}Te were populated using the ^{58}Ni(^{54}Fe,$2pn$) reaction. The ^{54}Fe beam was accelerated onto a 1-mg/cm^2 self-supporting ^{58}Ni target at a beam energy of 206 MeV over a period of two weeks, with an average beam intensity of 2.5 pnA. Prompt γ-ray transitions were observed in the PRE-JUROGAM II spectrometer [14] comprising 12 four-way segmented Clover detectors at a backward angle of 104.5° to the beam line and 15 single-crystal Ge detectors at backward angles of 158° and 134°. A downstream 1-mg/cm^2 Mg degrader foil, housed within the Köln plunger [15], reduced the full velocity of the recoiling fusion-evaporation residues from $v/c = 0.038(1)$ to 0.025(3). The Recoil-Ion Transport Unit (RITU) [16,17] separated the beamlike nuclei from the recoiling reaction products while transporting the latter to the GREAT focal-plane spectrometer [18]. Nuclei were implanted into a pair of double-sided silicon strip detectors (DSSD), the signal from which was used as a trigger for the creation of an event in the software. The energies of events occurring in all detectors were time stamped by a 100-MHz clock through the triggerless total data readout (TDR) acquisition system [19]. Decays measured in the PRE-JUROGAM II spectrometer were then correlated with signals detected at the focal plane through conditions imposed on the time of flight (ToF) of the recoils between the multiwire proportional counter (MWPC), at the entrance to GREAT, and the focal plane. Under the right experimental conditions, the high granularity of the DSSD can allow any subsequent nuclear decays to be measured and associated with the preceding nucleus from which the decay occurred. However, this technique of recoil decay tagging (RDT) [20] requires that the half-life of the measured decay is significantly smaller than the average nuclear implantation rate into the DSSD. In the case where this condition is not satisfied, random "false" coincidences will be measured. Due to the long half-life of the ^{109}Te α decay, 4.6(3) s [21], compared with the average DSSD implantation rate in this experiment of ∼4 kHz, it was not possible to cleanly identify and correlate delayed decays with their parent nucleus. Consequently, only recoil-gated data were collected for the analysis of ^{109}Te in this work. Recoil-gated data were collected for eight different target-to-degrader distances of 9.0(1), 73(1), 101(3), 215(5), 415(5), 500(4), 801(6), and 1995(25) μm and prepared for off-line sorting with the GRAIN software package [22]. The data were sorted into two-dimensional asymmetric spectra (matrices) for analysis with the UPAK [23] software suite.

III. ANALYSIS AND RESULTS

In order to isolate clean gating transitions in ^{109}Te it was necessary to identify the main evaporation channels in the fusion-evaporation reaction through the measurement of the relative yields of the observed γ-ray transitions. The relative yields were determined for the ^{54}Fe + ^{58}Ni reaction at a beam energy of 206 MeV from an analysis of a recoil-gated γ-γ coincidence matrix using the ESCL8R [24] analysis package. The matrix was constructed from data collected at the shortest target-to-degrader distance of 9 μm, where the majority of nuclei will have traversed the degrader foil before decaying. Table I shows the relative yields of the most intense channels observed in this work, normalized to the yield of ^{109}Sb ($3p$), the strongest exit channel. Each exit channel was identified using the previous knowledge of known γ-ray transitions in the residual nuclei. Only nuclei identified with a normalized yield >1% are included.

TABLE I. Experimental relative yields of the strongest evaporation channels measured in the ^{54}Fe + ^{58}Ni reaction at 206 MeV. These yields were derived from a fit to the ground-state transitions of each nucleus in the recoil-gated prompt γ-γ matrix.

Nucleus	Channel	Relative yield (%)
^{109}Sb	$3p$	100 ± 18
^{108}Sb	$3pn$	22 ± 3
^{108}Sn	$4p$	26 ± 4
^{109}Te	$2pn$	19 ± 4
^{106}Sn	$\alpha 2p$	19 ± 3
^{105}In	$\alpha 3p$	18 ± 3
^{110}Te	$2p$	5 ± 1

In order to determine the lifetimes of the excited states in ^{109}Te, the differential decay curve method (DDCM) was used in the γ-ray coincidence mode [25–27]. Within this method the lifetime of the measured state is determined at each target-to-degrader distance using the relation

$$\tau(x) = \frac{\{C, A_d\} - \alpha\{C, B_d\}}{\frac{d}{dx}\{C, A_s\}} \frac{1}{\langle v \rangle}. \quad (1)$$

Here, the quantities given in braces correspond to the number of coincident events for the fully Doppler-shifted, s, and degraded, d, components of the γ-ray transitions under investigation. In this coincident scheme, it is assumed that transition A depopulates the level of interest, which is directly fed by the transition B. A gate is placed on a higher lying transition C, which allows only one feeding path to the level A. The terms $\{C, A_s\}$, therefore, refer to the normalized intensity of the shifted component of the transition A after a gate has been placed on the transition C. The value of α accounts for the presence of more than one decay out of the state of interest, including any unobserved decays. The average recoil velocity of the compound nuclei is given by $\langle v \rangle$. Typically, gates are placed solely on the shifted component of a transition. However, the geometry of the PRE-JUROGAM II spectrometer necessitated gating on transitions observed in detectors of ring 3, located at 104.5° to the beam line. The inability to discern both the fully Doppler-shifted and degraded components of a γ-ray transition at this angle required gates to be placed across the full widths of the transitions C. Placing gates in this way introduces an element of background into the measured intensities of each peak, A and B. However, provided that both the feeding and depopulating transitions are included in the analysis, this element of background can be eliminated [27–29].

The final lifetime value of the excited state was determined from a weighted average of the individual values measured at each distance, x. To minimize the errors on the final lifetimes,

the average was calculated from only points that lie within the so-called region of sensitivity, the measured values that cover the particular range where the denominator and numerator in Eq. (1) reach their maximum values simultaneously. As the error associated with each measurement is derived from the absolute values of the quantities A, data taken from within this region will result in relatively small errors. It is also important to note that, within the DDCM, only the relative target-to-degrader distances are required.

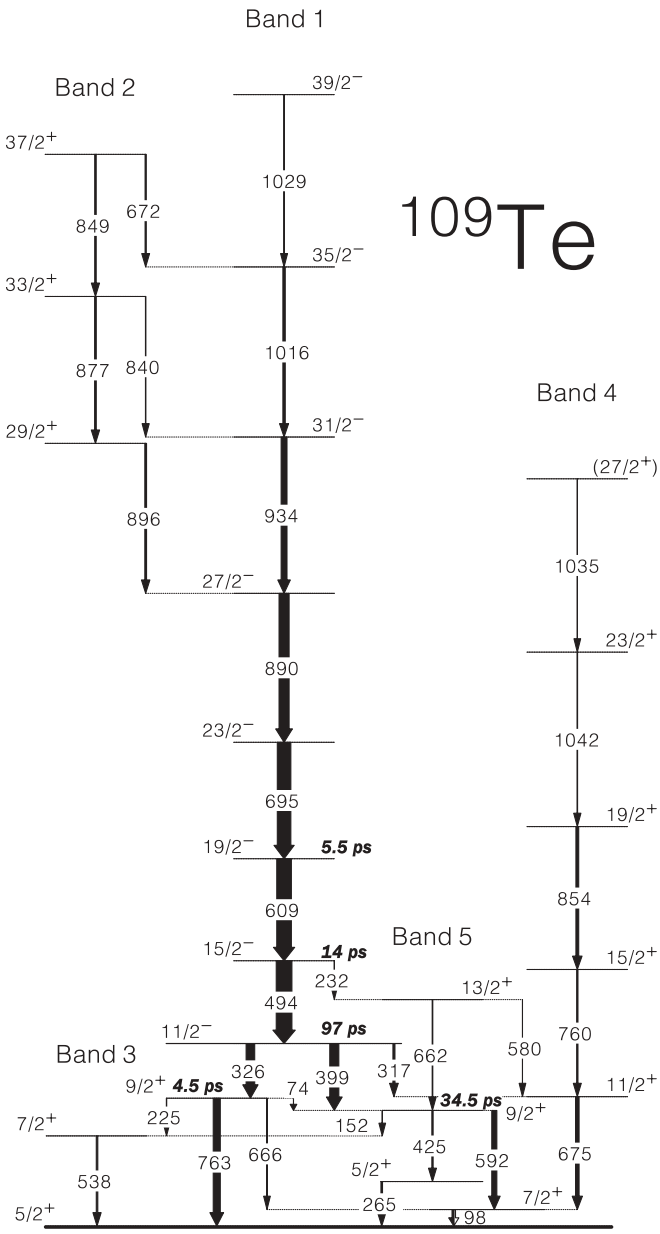

FIG. 1. Partial level scheme of ^{109}Te showing the transitions observed in this work. The transition energies are given in keV with the relative intensities given by the width of the arrows. The intensities were determined from γ-γ coincidence data collected at the shortest target-to-degrader distance, 9 μm where the majority of transitions are observed to reside in the Doppler-degraded component of the photopeak. The lifetimes of the states measured in this work are shown in bold text.

In this work, lifetime measurements have been made for several states at higher and lower excitation energy with respect to the first excited $\nu h_{11/2}$ level in ^{109}Te. Figure 1 shows a partial level scheme of ^{109}Te determined in this work, which is consistent with the level scheme previously published in Ref. [5]. The level scheme was constructed from data collected at the shortest of target-to-degrader distances, 9.0(1) μm, in ring 2 of the PRE-JUROGAM II spectrometer. At this distance the majority of transitions will occupy only the degraded component of the full photopeak. As such, applying a Doppler correction to the degraded velocity of the recoiling reaction products allowed a symmetric recoil-gated γ-γ matrix to be constructed for the analysis of the levels in ^{109}Te. Table II

TABLE II. Measured energies and intensities for transitions in ^{109}Te observed in this work.

E_γ(keV)[a]	I_γ[b]	Band	J_i^π	→	J_f^π	Multipolarity[c]
74	<1	5	$9/2^+$	→	$9/2^+$	
98.2	12.9	4	$7/2^+$	→	$5/2^+$	$M1/E2$
152.4	<1	5 → 3	$9/2^+$	→	$7/2^+$	
225.0	7.1	3	$9/2^+$	→	$7/2^+$	$M1/E2$
232	<1	1 → 5	$15/2^-$	→	$13/2^+$	
265.0	10	5	$5/2^+$	→	$5/2^+$	$M1/E2$
317.0	12.9	1 → 4	$11/2^-$	→	$11/2^+$	$E1$
326.0	55	1 → 3	$11/2^-$	→	$9/2^+$	$E1$
399.0	58.2	1 → 5	$11/2^-$	→	$9/2^+$	$E1$
424.8	8.1	5	$9/2^+$	→	$5/2^+$	$E2$
494.4	100	1	$15/2^-$	→	$11/2^-$	$E2$
538.0	2	3	$7/2^+$	→	$5/2^+$	$M1/E2$
580.0	<1	5 → 4	$13/2^+$	→	$11/2^+$	
592.4	32	5 → 4	$9/2^+$	→	$7/2^+$	$M1/E2$
609.0	94	1	$19/2^-$	→	$15/2^-$	$E2$
662.0	<1	5	$13/2^+$	→	$9/2^+$	$E2$
665.8	<1	3 → 4	$9/2^+$	→	$7/2^+$	
672.2	7.8	2 → 1	$37/2^+$	→	$35/2^-$	$E1$
675.0	23	4	$11/2^+$	→	$7/2^+$	$E2$
695.0	87	1	$23/2^-$	→	$19/2^-$	$E2$
760.3	8	4	$15/2^+$	→	$11/2^+$	$E2$
763.0	45	3	$9/2^+$	→	$5/2^+$	$E2$
839.9	2.7	2 → 1	$33/2^+$	→	$31/2^-$	$E1$
848.5	9.4	2	$37/2^+$	→	$33/2^+$	$E2$
853.8	17.8	4	$19/2^+$	→	$15/2^+$	$E2$
877.3	10.5	2	$33/2^+$	→	$29/2^+$	$E2$
889.6	65	1	$27/2^-$	→	$23/2^-$	$E2$
895.9	11.3	2 → 1	$29/2^+$	→	$27/2^-$	$E1$
933.7	37.5	1	$31/2^-$	→	$27/2^-$	$E2$
1015.7	15.2	1	$35/2^-$	→	$31/2^-$	$E2$
1029.4	1.7	1	$39/2^-$	→	$35/2^-$	$E2$
1035.3	3	4	$(27/2^+)$	→	$23/2^+$	
1042.4	3.7	4	$23/2^+$	→	$19/2^+$	$E2$

[a]For strong transitions, $I_\gamma > 10$ γ-ray energies are estimated to be accurate to ± 0.3 keV, and for weaker transitions they are estimated to be accurate to ± 0.6 keV. Energies quoted as integers are accurate to ± 1 keV.

[b]For strong transitions, $I_\gamma > 10$ the errors in the relative γ-ray intensities are estimated to be less than 10%, and for weaker transitions they are estimated to be less than 20%.

[c]Multipolarities taken from angular-distribution measurements performed in Ref. [5].

summarizes the energies and intensities measured for each of the transitions in ^{109}Te observed in this work.

Lifetimes were determined by fitting the fully Doppler-shifted and degraded components of each measured photopeak from data collected in rings 1 (five detectors) and 2 (ten detectors) of the PRE-JUROGAM II spectrometer at backward angles of 158° and 134° to the beam line, respectively, after placing gates on higher lying transitions observed in ring 3 at an angle of 104.5°.

A. States feeding the $\nu h_{11/2}$ level

Figure 2(a) shows an example of the data collected in ring 2 at three target-to-degrader distances for the 494-keV $15/2^- \rightarrow 11/2^-$ transition in band 1 (Fig. 1). The spectra were obtained from a gate on the full width of the higher lying 695-keV transition. The 890-keV transition was not included in the gate due to the presence of coincident 496- and 890-keV transitions in ^{108}Sb [30], which was also produced in the reaction used in this experiment. The positions of the fully Doppler-shifted and degraded peaks have been highlighted. The degraded component of the photopeak was observed to be fully populated at a distance of 100.5 μm, and the fully Doppler-shifted component is wholly populated at a distance of 801.2 μm. The three intermediate distances were observed to have both components of the photopeak present. Given the extremely weak relative intensity (<1%) measured in this work for the 232-keV transition, also depopulating the $15/2^-$ state, it was reasonable to neglect the intensity contribution from this decay path in the measurement of the $15/2^-$ state. Figure 2(b) shows representative spectra for the 609-keV transition feeding the $15/2^-$ state in the $\nu h_{11/2^-}$ band. The spectra were obtained after placing a gate on the full width of the higher lying 890-keV transition.

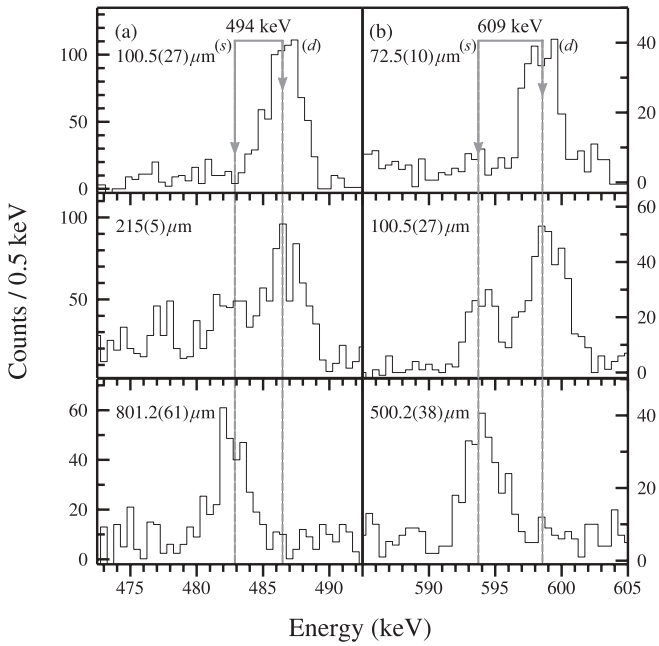

FIG. 2. Example of recoil-gated γ-γ coincidence spectra for three target-to-degrader distances for panel (a), the 494- and panel (b), the 609-keV transitions in ^{109}Te. The 494-keV gated spectra were produced from a gate on the higher-lying 695-keV γ ray. The 609-keV gated spectra were collected from an energy gate on the higher-lying 890-keV transition. The fully Doppler-shifted, (*s*) and degraded, (*d*) components of each transition have been highlighted. No Doppler correction has been applied to the spectra.

These spectra highlight the shifting of the full photopeak at a target-to-degrader distance of 72.5 μm with the fully Doppler-shifted component almost fully populated at 500.2 μm. A lack of statistics prevented the use of any higher spin gating transitions in the measurement of the $19/2^-$ and $15/2^-$ states. Sufficient data were present to allow the lifetime of the $15/2^-$ state to be independently determined from data collected in ring 1; however, a lack of statistics prevented the measurement of the lifetime of the $19/2^-$ state from ring 1 data. The normalized shifted intensities for the 495- and 609-keV transitions are shown in Fig. 3. Table III gives the final lifetime values determined for the excited states in ^{109}Te measured in this work.

B. The $\nu h_{11/2}$ band-head level

Figures 4(a) and 4(b) show representative spectra at three target-to-degrader distances for the 399- and 326-keV transitions depopulating the $\nu h_{11/2}$ band-head level in ^{109}Te, respectively. The spectra were obtained from a summation of energy gates placed upon the higher lying 695- and 609-keV transitions. Both spectra for the 399- and 326-keV transitions highlight the long-lived nature of the $\nu h_{11/2}$ level compared with the higher lying transitions that feed it. Even at the largest target-to-degrader separation of 1995 μm, a fraction of the full photopeak intensity still remains in the degraded component. The large separation between the normalized shifted components of the 399- and 326-keV transitions and that of the feeding transition allows for a more accurate determination of the final lifetime value of the $\nu h_{11/2}$ level.

Figure 4(b) also shows the less intense 317-keV transition, which depopulates the $\nu h_{11/2}$ level. It was not possible to measure the relative intensities of each component of the photopeak for this transition due to a lack of statistics as well as the presence of coincident 696- and 317-keV transitions in ^{105}In [31], also produced in the reaction used in this work. The measured lifetimes for both the 399- and 326-keV transitions, determined from data collected in both rings 1 and 2 of the PRE-JUROGAM II spectrometer, are given in Table II and are consistent with each another.

C. Transitions depopulating the $\nu h_{11/2}$ band-head level

Figure 5(a) shows representative spectra at three target-to-degrader distances for the 763-keV transition feeding the $5/2^+_1$ ground-state level in ^{109}Te. The spectra were produced from a summation of energy gates on the higher lying 494-, 609-, 695- and 890-keV transitions in band 1. The influence of the longer lived $\nu h_{11/2}$ level is evident in these spectra and the decay curves shown in Fig. 3 as the fully Doppler-shifted component begins to show only at a distance >200 μm. At the maximum target-to-degrader separation of 2000 μm only ~80% of the full photopeak intensity resides in the fully Doppler-shifted

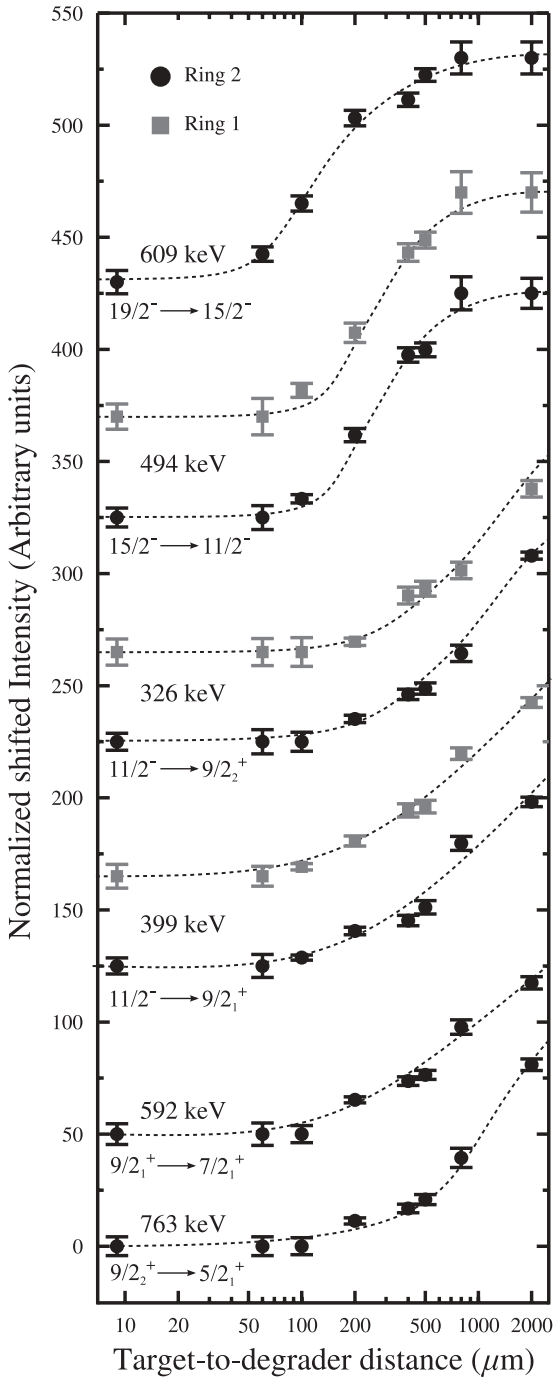

FIG. 3. Normalized shifted intensities for the transitions in ^{109}Te measured in this work. Square data points correspond to measurements from Ring 1 and circle data points measurements from Ring 2. The errors are derived solely from the statistical uncertainty in the intensity measurement of the two components of each photopeak. The dashed curves are drawn to guide the eye.

component. The large error associated with the lifetime measurement of the $9/2_2^+$ state, given in Table II, results from the small difference in the normalized shifted intensities of the 399-keV transition feeding this state and the 763-keV transition. This is a consequence of the large difference in lifetimes of the $\nu h_{11/2^-}$ band-head level and the $9/2_2^+$ state. In such a case, the ability to accurately fit the numerator in Eq. (1) requires a small statistical uncertainty on the intensity measurements of each component of the photopeak. Given the fragmentation of the total intensity feeding the yrast $\nu h_{11/2}$ level into several different parallel branches, insufficient statistics were available to more accurately separate the decay curves of the feeding and depopulating transitions. Figure 5(b) shows three spectra for the 592-keV transition obtained from the same summation of gates as those in Fig. 5(a). Figure 2 shows that these gates do not provide a unique feeding path to the $9/2_1^+$ state depopulated by the 592-keV γ ray transition. However, the intensities of the 662- and 74-keV transitions, which provide parallel routes to the $9/2_1^+$ state, were observed in this work to have normalized intensities $<1\%$. As such they were assumed to have little effect on the measured lifetime of the $9/2_1^+$ state within its given uncertainties. The intrinsic lifetime of the $9/2_1^+$ state, given in Table II, is larger than that of the $9/2_2^+$ state, and consequently the separation of the normalized-shifted components of the transitions feeding and depopulating this state was more obvious. This resulted in a smaller percentage error on the lifetime measurement of the $9/2_1^+$ state compared with that of the $9/2_2^+$ state.

IV. DISCUSSION

Reduced transition probabilities, $B(\sigma L)$, have been deduced from the experimentally measured lifetimes using the relationships

$$B(E1) = \frac{1}{\tau(1+\alpha)1.59 \times 10^{15} E_\gamma^3},$$

$$B(E2) = \frac{1}{\tau(1+\alpha)1.22 \times 10^{9} E_\gamma^5},$$

and

$$B(M1) = \frac{1}{\tau(1+\alpha)1.76 \times 10^{13} E_\gamma^3}, \quad (2)$$

where the lifetimes τ are given in ps, E_γ in MeV, $B(EL)$ in e^2 fm^{2L}, and $B(ML)$ in μ_N^2 fm^{2L-2}. The internal conversion coefficients α were taken from Ref. [32]. The $B(\sigma L)$ values assume pure-stretched transitions with no mixing from higher order multipolarities.

In order to interpret the experimental reduced transition probabilities, shell-model calculations have been performed using the realistic charge-dependent one-boson-exchange nucleon-nucleon (CD-Bonn) potential [33], renormalized using the perturbative G-matrix approach [34]. Calculations were made using a proton-neutron model space consisting of the $0g_{7/2}$, $1d_{5/2}$, $1d_{3/2}$, $2s_{1/2}$, and $0h_{11/2}$ orbitals. The corresponding single-particle energies of the neutron $g_{7/2}$ and $d_{5/2}$ orbitals were taken to be 0.0 and 0.172 MeV [35], respectively. The single-particle energies of the remaining states, as well as the $T = 1$ part of the monopole interaction, were determined using a global optimization method [36] by fitting to 157 low-lying yrast states in a range of $Z = 50$ tin nuclei between $102 < A < 132$. The optimized interaction has been observed to reproduce the experimental data within an average deviation of 130 keV. The $T = 0$ part of the monopole interaction is

TABLE III. Experimentally measured lifetime values, τ for excited states in ^{109}Te measured in this work. The energies of transitions depopulating the measured states and those on which gates were placed are given. Lifetime values are quoted for both rings 1 and 2 with the weighted average (WA) of each measurement also given.

J_i^π	J_f^π	$E_x(J_i^\pi)$ (keV)	E_γ (keV)	E^{gate} (keV)[a]	Lifetime (ps)			
					τ (ring 2)	τ (ring 1)	τ (WA)	τ (partial)
$19/2^-$	$15/2^-$	2192	609	890	5.5(13)	–	5.5(13)	5.5(13)
$15/2^-$	$11/2^-$	1583	494	695	14.7(18)	12.9(22)	14.0(14)	14(1)
$11/2^-$	$9/2_1^+$	1089	399	695,609	89.4(61)	98.2(59)	94(4)	210(16)[b]
$11/2^-$	$9/2_2^+$	1089	326	695,609	98.2(64)	106(7)	102(5)	222(18)[b]
$11/2^-$	$11/2_1^+$	1089	317	–	–	–	–	951(107)[b]
$9/2_1^+$	$7/2_1^+$	690	592	494,609,695,890	34.5(72)	–	34.5(72)	43(9)[c]
$9/2_1^+$	$5/2_2^+$	690	425	–	–	–	–	172(47)[c]
$9/2_2^+$	$5/2_1^+$	763	763	494,609,695,890	4.5(29)	–	4.5(29)	5(3)[d]
$9/2_2^+$	$7/2_2^+$	763	225	–	–	–	–	33(22)[d]

[a]Gates were placed across the full width of the γ-ray photopeak in ring 3 of the PRE-JUROGAM II spectrometer.
[b]Partial lifetimes derived from a weighted average of the individual measurements for the 399- and 326-keV transitions, 97(3) ps.
[c]Partial lifetimes derived under the assumption that the 152-keV transition has a negligible intensity, <1%.
[d]Partial lifetimes derived under the assumption that both the 666- and 74-keV transitions have negligible intensities, <1%.

not optimized due to computational limitation; the dimension around the midshell is currently too large to handle when both protons and neutrons are present. The calculations assumed isospin symmetry and the proton single-particle energies were taken to be the same as those for the neutrons.

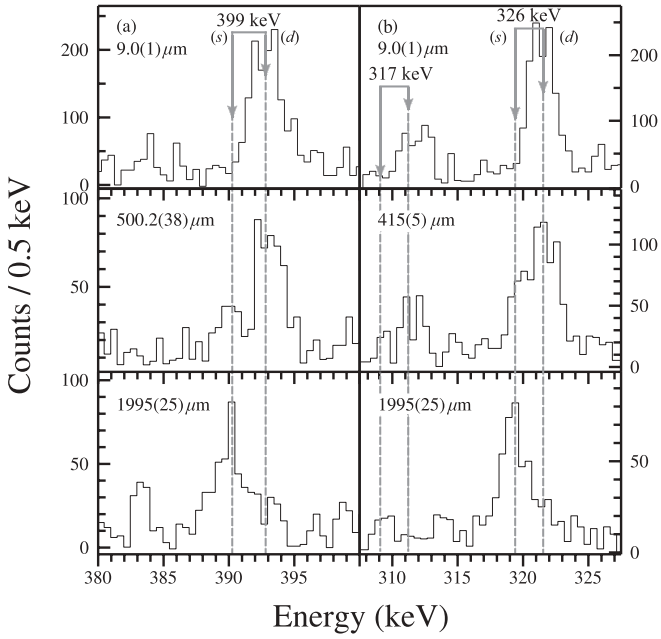

FIG. 4. Example of recoil-gated γ-γ coincidence spectra for three target-to-degrader distances for panel (a), the 399- and panel (b), the 326-keV transitions in ^{109}Te. The 326- and 399-keV peaks were measured after a summation of gates placed on the higher-lying 695- and 609-keV transitions. The fully Doppler-shifted, (s) and degraded, (d) components of each transition have been highlighted. Panel (b) also highlights the expected positions of the fully Doppler shifted and degraded components of the 317-keV γ ray. No Doppler correction has been applied to the spectra.

A. States feeding the $\nu h_{11/2}$ level

The structure of bands built upon the $\nu h_{11/2}$ orbital are well known in the majority of neutron-deficient odd-mass Te isotopes. These structures are interpreted as the favored signatures of the neutron $h_{11/2}$ band, resulting from the coupling of the odd valence neutron to the even-even tellurium core. Figure 6 compares the energies of the first excited states in

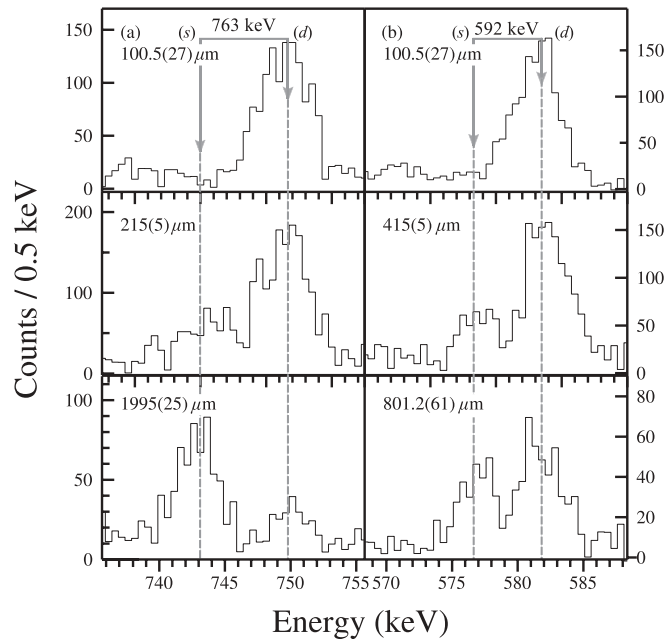

FIG. 5. Example of recoil-gated γ-γ coincidence spectra for three target-to-degrader distances for panel (a), the 763- and panel (b), the 592-keV transitions in ^{109}Te. The 753- and 592-keV peaks were measured after a summation of gates placed on the higher-lying 494-, 609-, 695- and 890-keV transitions. The fully Doppler-shifted, (s) and degraded, (d) components of each transition have been highlighted. No Doppler correction has been applied to the spectra.

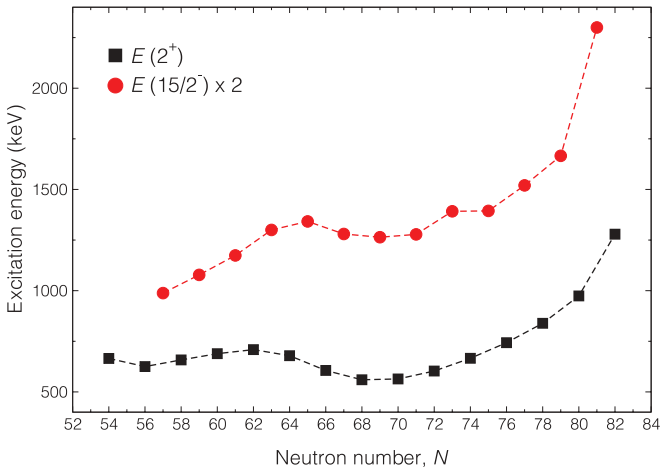

FIG. 6. (Color online) Excitation energies of the first excited states in the ground-state bands of the even-mass tellurium isotopes (squares) and the $\nu h_{11/2}$ bands (circles) of the odd-mass tellurium isotopes (relative to the $11/2^-$ band-head). Energies in the odd-mass isotopes have been multiplied by a factor of two to separate them from those of the even-mass isotopes. Data were taken from Refs. [5–8,37–43].

the $\nu h_{11/2}$ bands for $N < 82$ with their counterpart even-even ground-state configurations. The excitation energies of the states within the $\nu h_{11/2}$ bands follow the same trend as those in the more extensively studied even-mass tellurium ground-state configurations [8]. As the number of neutrons is reduced from midshell at $N = 66$ and the $N = 50$ closed shell is approached, the expected trend of increased single-particle-like behavior is not observed. The energy of the first excited state does not continue to increase as expected, in contrast to the situation when the $N = 82$ shell closure is approached. Instead, an increase in collective behavior is observed for $N < 62$, where the $E(2^+)$ energy begins to reduce. The expected increasing trend of the $E(2^+)$ energy is then restored again at ^{106}Te; see Fig. 6. Although the behavior exhibited by states in the $\nu h_{11/2}$ bands of the odd-mass tellurium isotopes appears to mimic this behavior, a lack of experimental knowledge for nuclei with $N < 57$ precludes any change toward single-particle behavior from being examined.

TABLE IV. Experimental and theoretical reduced transition probabilities, $B(E2)$ for the negative parity states in ^{109}Te. The theoretical $B(E2)$ values have been calculated using standard proton and neutron effective charges of $e^{\pi}_{\rm eff} = 1.5e$ and $e^{\nu}_{\rm eff} = 0.5e$, respectively.

$J^{\pi}_i \rightarrow J^{\pi}_f$	$B(E2)$ (e^2 fm^4)		$B(E2)$ (W.u.)	
	Exp.	CD-Bonn	Exp.	CD-Bonn
$15/2^- \rightarrow 11/2^-$	1982(142)	1099	64(5)	36
$19/2^- \rightarrow 15/2^-$	1771(419)	1116	57(13)	36
$23/2^- \rightarrow 19/2^-$	–	1077	–	35
$27/2^- \rightarrow 23/2^-$	–	995	–	32

The theoretically predicted excitation energies for the states in the $\nu h_{11/2}$ band of ^{109}Te are shown in Fig. 7. The excitation energies predicted from theory provide a reasonable match with the experimentally observed band structure, with the largest discrepancy arising at $15/2^-$ for the first excited state in the band. The theoretical calculations also predict the presence of a considerable deformed component in the structure of the band. This might suggest that any changes toward a more seniority-like scheme must present itself closer to the $N = 50$ magic shell closure. Further theoretical calculations are required in both the heavier-mass isotones and closer to the drip line in order to assess the trend of decreasing excitation energies for all levels within the $\nu h_{11/2}$ bands. The knowledge of experimental $B(E2)$ values for the excited states within the $\nu h_{11/2}$ bands is somewhat limited. Table IV shows the experimental $B(E2)$ values determined from the partial lifetime values of states above the $\nu h_{11/2}$ level in ^{109}Te measured in this work. Theoretical $B(E2)$ values, calculated with standard proton and neutron effective charges of $1.5e$ and $0.5e$, respectively, are also shown.

The theoretical reduced transition probabilities are observed to underestimate the experimental values by almost a factor of two. A recent paper by Bäck *et al*. [44] examined

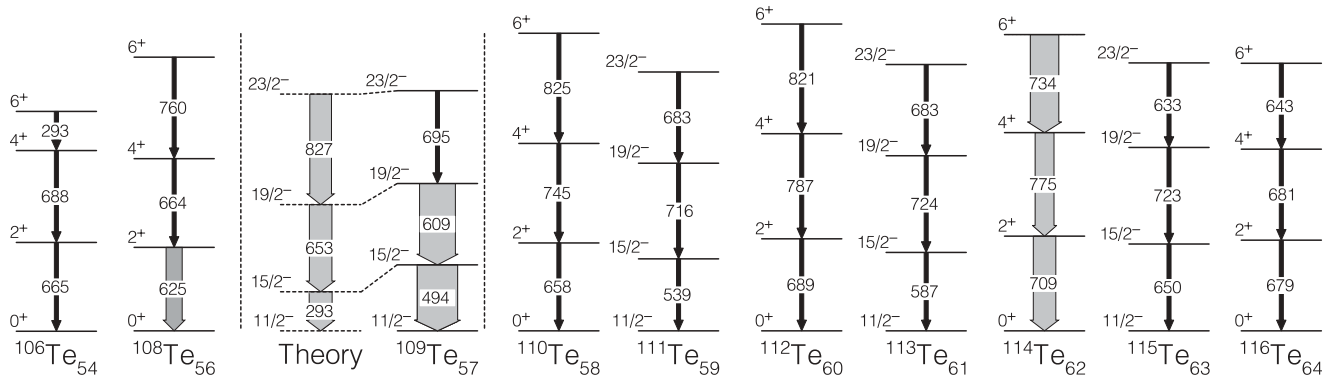

FIG. 7. Experimental excitation energies in the $\nu h_{11/2}$ bands of odd-mass tellurium nuclei for $N < 63$ compared with their even-even ground-state counterparts. Theoretical CD-Bonn calculations for ^{109}Te are also shown to the left of the experimental measurements. For states with experimentally measured $B(E2)$ values, the width of the shaded arrows denotes the strength of the decay normalised to the $15/2^- \rightarrow 11/2^-$ $B(E2)$ value in ^{109}Te. It should be noted that the ordering of the γ-ray transitions in ^{106}Te is tentative. The data for each of the tellurium isotopes are taken from [5–8,44–48]. States built upon the $\nu h_{11/2}$ level in ^{107}Te are yet to be observed.

the systematics of the ground-state $B(E2)$ values across the entire midshell chain in neutron-deficient even-mass tellurium isotopes. In that work it was observed that a neutron effective charge of $0.8e$ was required in order to best reproduce the experimental data across all of the measured isotopes. Using this information, the theoretical $B(E2)$ values have been recalculated for ^{109}Te using a neutron effective charge of $0.8e$. Within this approach the $B(E2)$ values for the $15/2^-$ and $19/2^-$ decays are calculated to be 1681 and 1708 e^2 fm^4, respectively, giving much closer agreement to the experimentally measured values in this work. However, the exact nature of the behavior of effective charges as the proton drip line is approached is not very well understood [11,49]. Despite this, the magnitude of the experimental and theoretical $B(E2)$ values points to a significant amount of collectivity within the band, as shown in Table IV. This result in itself is somewhat hard to resolve given the vibrational nature of the states built upon the single-neutron $\nu h_{11/2}$ configuration; the normalized energy ratios of the excited states in this band are consistently below 2.2. This anomaly is further highlighted by the constancy in the $B(E2)$ values as a function of increasing spin, observed both experimentally and theoretically. The large reduced transition probabilities, also observed in analogous bands of the measured even-mass tellurium isotopes, may be understood to arise from an enhanced contribution to the matrix elements from proton-neutron pairing. This description was used to interpret the increased collectivity in the ground-state sequences of the even-A Te isotopes inferred from energy systematics [6,8,9]. In the most neutron-deficient isotopes of tellurium, both protons and neutrons are predicted to occupy the same $d_{5/2}$ and $g_{7/2}$ orbitals. This results in a maximized overlap of the proton-neutron wave functions, leading to highly correlated p-n pairs. One of the consequences of this coupling scheme is a predicted enhancement of collective nuclear behavior. A similar trend of increasing collectivity as the $N = 50$ shell closure is approached is observed in the neutron-deficient xenon isotopes and has been attributed to the same shell-structure effect [50]. In comparison with the measured $B(E2)$ values in the ground-state sequences of the even-mass tellurium isotopes (see Fig. 7) the experimental $B(E2)$ values in the $\nu h_{11/2}$ band measured in this work are systematically larger. Spectroscopy measurements on the heavier mass ^{111}Te isotope, coupled with core-quasiparticle coupling calculations, pointed to a deformation driving force exerted by the valence $h_{11/2}$ neutron on the soft even-even core [6]. However, the possibility of a nonzero spectroscopic quadrupole moment in the core itself would reduce the significance of this effect. Further lifetime measurements in the $\nu h_{11/2}$ bands of the heavier odd-mass tellurium isotopes are required to further examine this changing nuclear behavior.

B. Lifetime of the $\nu h_{11/2}$ level

The lifetimes of the first excited $\nu h_{11/2}$ level are known in many of the neutron-deficient tellurium isotopes. In the majority of cases, for $A > 111$ the decay proceeds through an $M2$ transition linking the $\nu h_{11/2}$ level to the first excited $7/2^+$ state. In ^{109}Te, however, the decay from this level results in the emission of three $E1$ γ rays, populating excited states above the $5/2^+$ ground state. The presence of these additional decays results from the increase in energy of the $\nu h_{11/2}$ level with respect to the lower $9/2^+$ orbits around the Fermi surface, as the $N = 50$ shell closure is approached. This, coupled with the systematic studies of $E1$ transition strengths by Lobner and Malmskog [51,52], highlighting the wide range of expected $B(E1)$ values that result from the natural hindrance associated with $E1$ transitions undergoing a configuration change, precludes any comparison with previous measurements in the tellurium isotopes.

C. States depopulating the $\nu h_{11/2}$ level

Table V compares the experimental and theoretical excitation energies and reduced transition probabilities for the low-lying positive parity states in ^{109}Te. The theoretically predicted excitation energies, shown in Fig. 8, are able to successfully reproduce the staggering of the first excited states of each angular momentum. However, the second excited states for each angular momentum are systematically predicted to reside at higher energies than measured experimentally. However, the predicted reduced transition probabilities, shown in Table V, suggest that the ordering of the first two excited $9/2^+$ states may be inverted. This can be seen when comparing the experimental $B(E2)$ values for both the $9/2^+_1 \rightarrow 5/2^+_2$ and $9/2^+_2 \rightarrow 5/2^+_1$ transitions with the near-zero values predicted from the shell-model calculations. In contrast, the theoretical values predicted for the inband $E2$ decays from the $9/2^+_1$ and $9/2^+_2$ states appear to match well with those measured experimentally for the out-of-band transitions. No decays are

TABLE V. Experimental and theoretical reduced transition probabilities, $B(E2)$ for the low-lying positive-parity states in ^{109}Te. The theoretical $B(E2)$ values have been calculated using proton and neutron effective charges of $e^\pi_{\rm eff} = 1.5e$ and $e^\nu_{\rm eff} = 0.5e$, respectively.

$J^\pi_h \rightarrow J^\pi_h$	$E_x(J^\pi_i)$ (keV)		$B(E2)$ (e^2 fm^4)	
	Exp.	CD-Bonn	Exp.	CD-Bonn
$9/2^+_1 \rightarrow 5/2^+_1$	690	535	–	683
$9/2^+_1 \rightarrow 5/2^+_2$	690	535	340(93)	6
$9/2^+_2 \rightarrow 5/2^+_1$	763	1228	608(392)	12
$9/2^+_2 \rightarrow 5/2^+_2$	763	1228	–	407
$11/2^+_1 \rightarrow 7/2^+_1$	773	822	–	810
$11/2^+_2 \rightarrow 7/2^+_2$	1221	1581	–	650
$13/2^+_1 \rightarrow 9/2^+_1$	1352	1308	–	850
$13/2^+_2 \rightarrow 9/2^+_2$	–	2050	–	690
			$B(M1)$ (μ^2_N)	
	Exp.	CD-Bonn	Exp.	CD-Bonn
$7/2^+_1 \rightarrow 5/2^+_1$	98	214	–	0.151
$7/2^+_1 \rightarrow 5/2^+_2$	98	214	–	0.055
$7/2^+_2 \rightarrow 5/2^+_1$	538	882	–	0.002
$7/2^+_2 \rightarrow 5/2^+_2$	538	882	–	0.076
$9/2^+_1 \rightarrow 7/2^+_1$	690	535	0.006(1)	0.162
$9/2^+_1 \rightarrow 7/2^+_2$	690	535	–	0.126
$9/2^+_2 \rightarrow 7/2^+_1$	763	1228	–	0.000
$9/2^+_2 \rightarrow 7/2^+_2$	763	1228	0.137(92)	0.102

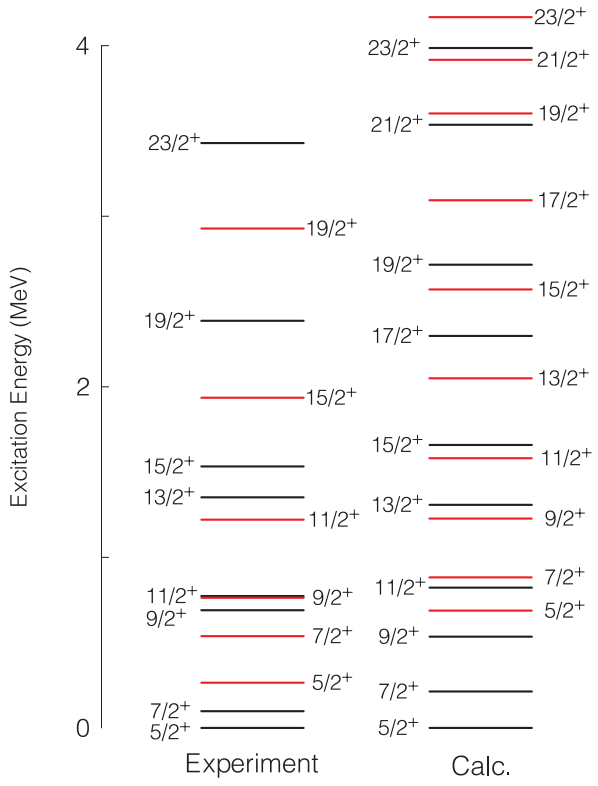

FIG. 8. (Color online) Experimental and theoretical excitation energies for the low-lying positive-parity states in ^{109}Te. Both the first and second (red) excited states for a given spin are shown.

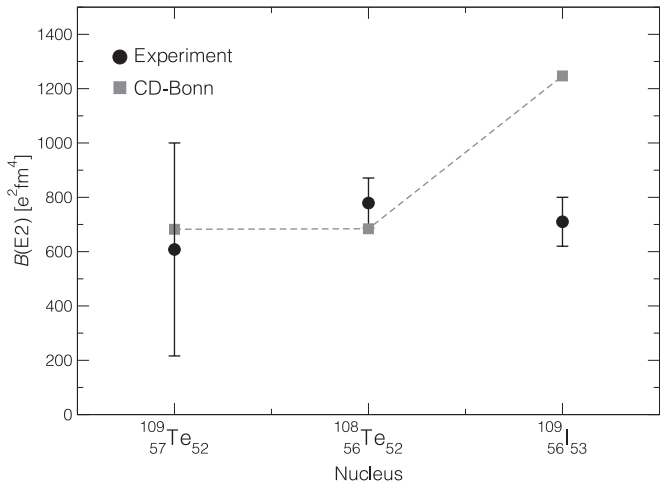

FIG. 9. Comparison of theoretical $B(E2)$ values, determined from shell-model calculations, with the experimentally measured values for the ground-state transitions in $^{109}_{52}$Te, $^{108}_{52}$Te and $^{109}_{53}$I. The theoretical values have been calculated with standard proton and neutron effective charges of $e_p = 1.5e$ and $e_n = 0.5e$, respectively.

experimentally established for the $9/2^+_1 \rightarrow 5/2^+_1$ and $9/2^+_2 \rightarrow 5/2^+_2$ transitions. Interpreting the theoretically predicted $9/2^+$ states as being inverted compared with the experimentally measured values also results in a better correspondence between the experimental and theoretical $B(M1)$ values for the $9/2^+_2 \rightarrow 7/2^+_2$ decay. This disagreement between the theory and experiment can be interpreted as arising from the strong configuration mixing of all the single-particle shell orbitals. The two $9/2^+$ states are seen to lie very close in energy experimentally, ~74 keV, and hence they likely comprise an admixture of the two calculated $9/2^+$ states, which are shown to be rather pure, decaying only to the first and second excited $5/2^+$ and $7/2^+$ states. In order to further address this potential configuration, mixing would require the observation of the extremely weak transitions linking the in band $9/2^+$ and $5/2^+$ states.

Figure 9 compares the experimental and theoretical $B(E2)$ values of the ground-state transitions in ^{109}Te, ^{108}Te [44], and ^{109}I [11]. This comparison assumes that the first two theoretically predicted $9/2^+$ states are inverted with respect to experimental measurements, as discussed above. Although the large error associated with the ^{109}Te measurement prevents any definitive conclusions from being drawn, it appears that the $B(E2)$ values determined from shell-model calculations performed in this work are able to successfully reproduce the low-lying decay characteristics of both tellurium isotopes. In contrast, the theoretical value for the proton-unbound nucleus ^{109}I overestimates the experimental value. This overestimation was deduced to result from the inability of shell-model calculations to correctly account for the unbound nature of valence nucleons [11,12]. While the comparison was performed using standard proton and neutron effective charges of $1.5e$ and $0.5e$, respectively, it was observed that such a dramatic change in the $B(E2)$ values between ^{108}Te and ^{109}I could not be resolved by a simple change of the effective charge. Instead the discrepancy was attributed to the decoupled nature of the valence proton. The unbound proton was assumed to have a significantly reduced contribution toward the total $B(E2)$ value, which shell-model calculations were unable to take account of. In order to further investigate these experimental observations, additional lifetime measurements are required in several other proton- and α-unbound nuclei, as well as their more stable neighboring isotopes.

V. CONCLUSIONS

In summary, lifetime measurements have been made for five excited states in the α-unbound nucleus ^{109}Te using the Köln plunger device coupled to the PRE-JUROGAM II–RITU-GREAT setup at the University of Jyväskylä, Finland. The experimental reduced transition probabilities have been compared to state-of-the-art shell-model calculations using the monopole-corrected CD-Bonn nucleon-nucleon potential. Excited states within the $\nu h_{11/2}$ band exhibit large $B(E2)$ values, further emphasizing the unexpected increase in deformation observed in the neutron-deficient tellurium isotopes as the $N = 50$ shell closure is approached. When compared with the analogous ground-state bands in the even-even tellurium cores, the larger $B(E2)$ values measured in this work are attributed to the deformation driving properties of the single valence neutron occupying the $\nu h_{11/2}$ shell. Experimental $B(E2)$ values for the low-lying positive-parity states were also compared to shell-model calculations, as well as recent

measurements in the neighboring nuclei ^{108}Te and ^{109}I. The potential mixing of the first two excited $9/2^+$ states alludes to the highly complicated nature of their wave functions, which involve large configuration mixing from both the $d_{5/2}$ and $g_{7/2}$ orbitals. The comparison with measurements in neighboring nuclei pointed to the differing contributions of valence proton and α particles to the total $B(E2)$ strengths of the ground-state decays. The shell-model calculations seem to overestimate the contribution from a decoupled proton to the total $B(E2)$ value. Further lifetime measurements of neutron-deficient odd-mass tellurium isotopes, as well as a range of α and proton-unbound nuclei, are required to further examine the structural changes in nuclei at the extremes of existence.

ACKNOWLEDGMENTS

This work has been supported by the EU Sixth Framework Programme, "Integrating Infrastructure Initiative Transnational Access," Contract No. 506065 (EURONS), and by the Academy of Finland under the Finnish Centre of Excellence Programme 2006–2011 (Nuclear and Accelerator Based Physics Programme at JYFL). The authors acknowledge the support of GAMMAPOOL for the loan of the JUROGAM detectors. M.G.P, D.M.C., and M.J.T acknowledge the support of the STFC through Contract No. ST/G008787/1. T.B., B.C., R.L., and C.Q. acknowledge the support of the Swedish Research Council under Grants No. 6621-2010-3694 and No. 621-2010-4723 and of the Nordic Infrastructure under NordForsk (Project No. 070315).

[1] H. C. Scraggs *et al.*, Phys. Rev. C **61**, 064316 (2000).
[2] T. Ishii, A. Makishima, M. Shibata, M. Ogawa, and M. Ishii, Phys. Rev. C **49**, 2982 (1994).
[3] E. S. Paul *et al.*, Phys. Rev. C **61**, 064320 (2000).
[4] B. Hadinia *et al.*, Phys. Rev. C **70**, 064314 (2004).
[5] A. J. Boston *et al.*, Phys. Rev. C **61**, 064305 (2000).
[6] K. Starosta *et al.*, Phys. Rev. C **61**, 034308 (2000).
[7] J. M. Sears *et al.*, Phys. Rev. C **57**, 1656 (1998).
[8] B. Hadinia *et al.*, Phys. Rev. C **72**, 041303 (2005).
[9] D. S. Delion, R. Wyss, R. J. Liotta, B. Cederwall, A. Johnson, and M. Sandzelius, Phys. Rev. C **82**, 024307 (2010).
[10] E. Caurier, F. Nowacki, A. Poves, and K. Sieja, Phys. Rev. C **82**, 064304 (2010).
[11] M. G. Procter *et al.*, Phys. Lett. B **704**, 118 (2011).
[12] M. G. Procter *et al.*, AIP Conf. Proc. **1409**, 105 (2011).
[13] P. J. Nolan and J. F. Sharpey-Schafer, Rep. Prog. Phys. **42**, 1 (1979).
[14] P. J. Nolan, F. A. Beck, and D. B. Fossan, Annu. Rev. Nucl. Part. Sci. **44**, 561 (1994).
[15] L. Cleemann *et al.*, Nucl. Instrum. Methods **156**, 477 (1978).
[16] M. Leino *et al.*, Nucl. Instrum. Methods Phys. Res., Sect. B **99**, 653 (1995).
[17] M. Leino, Nucl. Instrum. Methods Phys. Res., Sect. B **126**, 320 (1997).
[18] R. D. Page *et al.*, Nucl. Instrum. Methods Phys. Res., Sect. B **204**, 634 (2003).
[19] I. Lazarus *et al.*, IEEE Trans. Nucl. Sci. **48**, 567 (2001).
[20] E. S. Paul *et al.*, Phys. Rev. C **51**, 78 (1995).
[21] J. Blachot, Nucl. Data Sheets **86**, 505 (1999).
[22] P. Rahkila, Nucl. Instrum. Methods Phys. Res., Sect. A **595**, 637 (2008).
[23] W. T. Milner (private communication).
[24] D. C. Radford, Nucl. Instrum. Methods Phys. Res., Sect. A **361**, 297 (1995).
[25] A. Dewald, S. Harissopulos, and P. von Brentano, Z. Phys. A **334**, 163 (1989).
[26] G. Böhm, A. Dewald, P. Petkov, and P. von Brentano, Nucl. Instrum. Methods **329**, 248 (1993).
[27] A. Dewald, O. Möller, and P. Petkov, Prog. Part. Nucl. Phys. **67**, 786 (2012).
[28] A. Dewald *et al.*, Phys. Rev. C **68**, 034314 (2003).
[29] M. G. Procter *et al.*, Phys. Rev. C **81**, 054320 (2010).
[30] D. G. Jenkins *et al.*, Phys. Rev. C **58**, 2703 (1998).
[31] J. Kownacki *et al.*, Nucl. Phys. A **627**, 239 (1997).
[32] T. Kibédi *et al.*, Nucl. Instrum. Methods Phys. Res., Sect. A **589**, 202 (2008).
[33] R. Machleidt, Phys. Rev. C **63**, 024001 (2001).
[34] M. Hjorth-Jensen, T. T. S. Kuo, and E. Osnes, Phys. Rep. **261**, 125 (1995).
[35] I. G. Darby *et al.*, Phys. Rev. Lett. **105**, 162502 (2010).
[36] C. Qi (unpublished).
[37] C.-B. Moon *et al.*, Nucl. Phys. A **657**, 251 (1999).
[38] C. T. Papadopoulos *et al.*, Z. Phys. A **352**, 243 (1995).
[39] N. Blasi *et al.*, Z. Phys. A **352**, 359 (1995).
[40] N. Blasi *et al.*, Z. Phys. A **354**, 233 (1996).
[41] A. Kerek, J. Kownacki, A. Marelius, and J. Pihl, Nucl. Phys. A **194**, 64 (1972).
[42] C. T. Zhang *et al.*, Z. Phys. A **353**, 11 (1995).
[43] C. Zhang *et al.*, Nucl. Phys. A **628**, 386 (1998).
[44] T. Bäck *et al.*, Phys. Rev. C **84**, 041306 (2011).
[45] E. S. Paul *et al.*, Phys. Rev. C **76**, 034322 (2007).
[46] E. S. Paul *et al.*, Phys. Rev. C **50**, 698 (1994).
[47] O. Möller *et al.*, Phys. Rev. C **71**, 064324 (2005).
[48] C.-B. Moon *et al.*, Z. Phys. A **358**, 373 (1997).
[49] T. Engeland, M. Hjorth-Jensen, and E. Osnes, Phys. Rev. C **61**, 021302 (2000).
[50] M. Sandzelius *et al.*, Phys. Rev. Lett. **99**, 022501 (2007).
[51] K. E. G. Lobner, Phys. Lett. B **26**, 369 (1968).
[52] K. E. G. Lobner and S. G. Malmskog, Nucl. Phys. **80**, 505 (1965).